Pattern Recognition Letters 54 (2015) 18–26

Contents lists available at ScienceDirect

Pattern Recognition Letters

journal homepage: www.elsevier.com/locate/patrec

3D rotation invariants of Gaussian–Hermite moments ☆

Bo Yang [a,b], Jan Flusser [a], Tomáš Suk [a,*]

[a] Institute of Information Theory and Automation of ASCR, Pod Vodárenskou věží 4, 182 08 Praha 8, Czech Republic
[b] Northwestern Polytechnical University, 127 West Youyi Road, Xi'an Shaanxi, 710072, P.R. China

ARTICLE INFO

Article history:
Received 14 April 2014
Available online 13 December 2014

Keywords:
Rotation invariants
Orthogonal moments
Gaussian–Hermite moments
3D moment invariants

ABSTRACT

3D rotation invariants based on orthogonal Gaussian–Hermite moments are proposed in this paper. We present an elegant and easy theoretical derivation of them. At the same time we prove by experiments that the Gaussian–Hermite invariants have better numerical stability than the traditional invariants composed of geometric moments.

1. Introduction

Pattern classification and object recognition play vital roles in image processing and computer vision. Generally, recognition is achieved by seeking descriptors that can represent the object regardless of certain transformations and/or deformations. Moment invariants were proved to be very powerful tools for feature representation and it has been demonstrated many times that moment invariants perform effectively in object recognition [1].

So far, various kinds of moment invariants to spatial transformations of the object have been proposed. Among all transformations that have been studied in this context, *rotation* plays a central role. Being a part of rigid-body transformation, object rotation is present almost in all applications, even if the imaging system is well set up and the experiment has been prepared in a laboratory. On the other hand, rotation is not trivial to handle mathematically, unlike for instance translation and scaling. For these two reasons, invariants to rotation have been in focus of researchers since the beginning.

With the rapid progress of applied mathematics, computer science and sensor technology, 3D imaging comes into engineering and practice due to its more flexible and precise descriptions of 3D objects. Undoubtedly, developing rotation invariants for 3D images has become a hot topic in the computer vision community. However, 3D rotation is more difficult to handle than its 2D counterpart, since it has three independent parameters. That is probably why only few papers on 3D rotation moment invariants have appeared so far. The first attempts to derive 3D rotation moment invariants are relatively old. Sadjadi and Hall [2] explored ternary quadratics extensively and derived three translation, rotation and scaling (TRS) moment invariants. Guo [3] proved the results of Sadjadi and Hall in the different way and he derived more invariants to translation and rotation in 3D space. Cyganski and Orr [4] applied tensor theory to derive 3D rotation invariants. This method was also mentioned by Reiss [5], who used invariant image features to recognize planar objects. Xu and Li [6] developed the invariants in both 2D and 3D space based on geometric primitives, such as distance, area, and volume. Galvez and Canton [7] employed normalization approach. The object is transformed into the coordinates given by eigenvectors of the second-order moment matrix and its transformed moments are taken as invariants. A modification of this method appeared in [8], where a slightly different moment matrix is used for normalization. Another method to derive 3D rotation invariants is based on complex moments [9,10]. Recently, Suk and Flusser [11] proposed an automatic algorithm to generate 3D rotation invariants from geometric moments up to an arbitrary order.

Although moments are probably the most popular 3D shape descriptors, it should be mentioned that they are not the only features providing rotation invariance. For example, Kakarala and Mao [12] used the bispectrum well-known from statistics for feature computation. Kazhdan [13] used an analogy of phase correlation based on spherical harmonics for comparison of two objects. In this particular case it was used for registration, but can be also utilized for recognition. In [14], the authors used amplitude coefficients as the features. Fehr [15] used the power spectrum and bispectrum computed from a tensor function describing an object composed of patches. In [16], the same author employed local binary patterns and in [17] he used local spherical histograms of oriented gradients.

In comparison with traditional geometric or complex moments, the outstanding advantage of orthogonal moments is their better numerical stability, limited range of values, and existing recurrent relations for their calculation. Hence, several authors have tried to derive the 2D invariants from orthogonal moments. In 3D, however, the

☆ This paper has been recommended for acceptance by Andrea Torsello.

* Corresponding author. Tel.: +420 26605 2231; fax: +420 28468 0730.
E-mail address: suk@utia.cas.cz (T. Suk).

http://dx.doi.org/10.1016/j.patrec.2014.11.014
0167-8655/

situation is more difficult than in 2D, but one can still expect that 3D orthogonal moments preserve their favorable numerical properties. There exist polynomials orthogonal inside a unit ball and others that are orthogonal on a unit cube. Seemingly, the polynomials defined on a unit ball are more convenient for deriving rotation invariants because the ball is mapped onto itself and the polynomials are transformed relatively easily under rotation. This approach was used by Canterakis [18] who employed 3D Zernike moments.

In this paper, we propose rotation 3D invariants from Gaussian–Hermite moments. To derive them, we used an approach that we already successfully applied in 2D [19]. We prove that the transformation of Gaussian–Hermite moments under rotation can be deduced indirectly, without explicit investigation of this transformation. Under our knowledge, Gaussian–Hermite polynomials are the only ones offering this possibility. Hence, we prove in the paper that the rotation invariants from Gaussian–Hermite moments have the same forms as those of rotation invariants from geometric moments in 3D space. This is an important conclusion because it allows us to reduce rotation invariant derivation from Gaussian–Hermite moments to that from geometric moments in 3D space, which are much easier to develop but we still benefit from the numerical stability of Gaussian–Hermite moments.

The core idea of the paper and its main theoretical achievement expressed by Theorem 1 is similar to that presented in [19] for a 2D case. It should be, however, stressed that the transition from 2D to 3D is not generally straightforward and easy. The rotation in 3D has three degrees of freedom comparing to a single parameter of a 2D rotation. Hence, any 3D mathematical objects and structures somehow related to rotation are far more rich than in 2D. Another difference that also makes the 3D problem more complicated is that rotation in 3D is not commutative. These are the reasons why the generalization from 2D to 3D cannot be done automatically but should always be carefully studied. Such studies sometimes discover an analogy with 2D (which is the case of this paper) and sometimes end up with different results.

The rest of the paper is organized as follows. Section 2 gives a general introduction to 3D rotation. The latest achievement about rotation invariants from geometric moments in 3D space is also recalled in this section. Section 3 reviews Gaussian–Hermite moments and gives two theorems according to which we can use the formations of geometric invariants to build rotation invariants of Gaussian–Hermite moments. Numerical experiments are presented in Section 4. Finally, Section 5 concludes the paper.

2. 3D rotation and its invariants

To describe a rotation in 3D space, we use extrinsic Tait–Bryan angle convention $(z-y-x)$ [20]. We consider the rotation along z axis by angle α, along y axis by angle $-\beta$, and along x axis by angle γ. Hence, a general 3D rotation can be directly represented by a matrix multiplication

$$\mathbf{R} = \mathbf{R_x}(\gamma)\mathbf{R_y}(-\beta)\mathbf{R_z}(\alpha). \tag{1}$$

Any rotation in 3D space can be decomposed into three successive rotations as defined by Eq. (1). Thanks to this, it is sufficient to consider elementary rotations along the axes only.

In 3D space, geometric central moment of order $(p+q+r)$ is defined

$$\mu_{pqr} = \int_{-\infty}^{\infty}\int_{-\infty}^{\infty}\int_{-\infty}^{\infty}(x-x_c)^p(y-y_c)^q(z-z_c)^r f(x,y,z)\,dxdydz, \tag{2}$$

where the centroid of the image $f(x,y,z)$ is calculated by $x_c = m_{100}/m_{000}$, $y_c = m_{010}/m_{000}$, and $z_c = m_{001}/m_{000}$. Recently, Suk and Flusser [11] proposed and implemented an automatic method for generating 3D rotation invariants from geometric moments. Their complete results are summarized in [21]. A list of 1185 irreducible rotation invariants in 3D space is available there. These invariants are built up from the moments of order 2 up to order 16. 3D rotation invariants of geometric moments are potential tools for the applications, such as object recognition and image retrieval. However, poor numerical stability exposes when the order of the invariant increases to a certain number. Hence, it is necessary to develop 3D rotation invariants based on orthogonal moments, which generally have better numerical stability than geometric moments.

3. 3D rotation invariants from Gaussian–Hermite moments

3.1. Gaussian–Hermite moments

The pth degree Hermite polynomial is defined by

$$H_p(x) = (-1)^p \exp(x^2)\frac{d^p}{dx^p}\exp(-x^2). \tag{3}$$

Hermite polynomials can be efficiently computed by the following 3-term recurrence relation:

$$H_{p+1}(x) = 2xH_p(x) - 2pH_{p-1}(x) \quad \text{for } p \geq 1, \tag{4}$$

with the initial conditions $H_0(x)=1$ and $H_1(x)=2x$. Hermite polynomials are orthogonal on $(-\infty,\infty)$ with a Gaussian weight function

$$\int_{-\infty}^{\infty} H_p(x)H_q(x)\exp(-x^2)dx = 2^p p!\sqrt{\pi}\,\delta_{pq}, \tag{5}$$

where δ_{pq} is the Kronecker delta. A weighted and normalized version, which is actually a scaled Hermite function, is usually used in practice

$$\widetilde{H}_p(x;\sigma) = (2^p p!\sqrt{\pi}\sigma)^{-1/2}H_p(x/\sigma)\exp(-x^2/2\sigma^2). \tag{6}$$

Gaussian–Hermite moment is defined with (6) being its basis function. The system (6) is not only orthogonal but also orthonormal, so it is convenient to conduct image reconstruction from the corresponding moments. However, when we multiply $\widetilde{H}_p(x;\sigma)$ in x direction and $\widetilde{H}_q(y;\sigma)$ in y direction, the product depends not only on the sum $p+q$, but also on the product $p!q!$; therefore, we must remove it from the basis function

$$\widehat{H}_p(x;\sigma) = H_p(x/\sigma)\exp(-x^2/2\sigma^2). \tag{7}$$

Fig. 1 shows such non-coefficient basis functions (7) of order 8 with different σ. We call the moments with respect to the basis functions (7) non-coefficient Gaussian–Hermite moments. For an image $f(x,y,z)$ in 3D space, its non-coefficient Gaussian–Hermite moment of order $p+q+r$ is defined as

$$\eta_{pqr} = \int_{-\infty}^{\infty}\int_{-\infty}^{\infty}\int_{-\infty}^{\infty}\widehat{H}_p(x;\sigma)\widehat{H}_q(y;\sigma)\widehat{H}_r(z;\sigma)f(x,y,z)dxdydz. \tag{8}$$

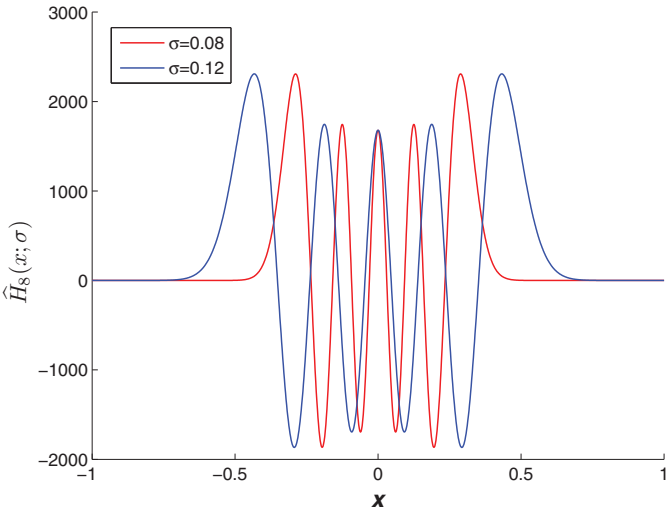

Fig. 1. Non-coefficient basis functions of the 8th order with different σ.

In general, we prefer to use the central Gaussian–Hermite moments to achieve the translation invariance

$$\overline{\eta}_{pqr} = \int_{-\infty}^{\infty}\int_{-\infty}^{\infty}\int_{-\infty}^{\infty} \widehat{H}_p(x - x_c;\sigma)\widehat{H}_q(y - y_c;\sigma)\widehat{H}_r(z - z_c;\sigma) f(x, y, z)dxdydz. \quad (9)$$

The choice of the actual σ value depends on the size of the object. It should be chosen such that the centralized basis functions (7) effectively cover the object.

3.2. Derivation of rotation invariants

Rotation invariants based on Gaussian–Hermite moments have been proposed for 2D image by Yang et al. [19] who showed that rotated Hermite polynomials are transformed in the same way as basic monomials $x^p y^q$. Here we formulate and prove an analogical theorem for a 3D case.

Theorem 1. *Let p, q, and r be three non-negative integers. Let the coordinates be rotated as* $(\hat{x}\ \hat{y}\ \hat{z})^T = \mathbf{R}(x\ y\ z)^T$. *Then*

$$\hat{x}^p\hat{y}^q\hat{z}^r = \sum_{i=1}^{L(p,q,r)} con_i\,(p, q, r, \alpha, \beta, \gamma)\, x^{p_i} y^{q_i} z^{r_i}, \quad (10)$$

where $L(p, q, r)$ *is a certain number determined by* p, q, r. con_i *represents a constant sequence specifically related to* p, q, r, α, β *and* γ. p_i, q_i, r_i *are integers determined by* p, q, r. *Hermite polynomials are transformed in the same way*

$$H_p(\hat{x})H_q(\hat{y})H_r(\hat{z}) = \sum_{i=1}^{L(p,q,r)} con_i\,(p, q, r, \alpha, \beta, \gamma)\, H_{p_i}(x)H_{q_i}(y)H_{r_i}(z). \quad (11)$$

The proof of Theorem 1 can be found in Appendix A. It is easy to prove that with the standard deviations $\sigma_x = \sigma_y = \sigma_z$, 3D Gaussian functions are rotation invariants when the transformation of coordinates is defined by (1). So, multiplying a 3D Gaussian function at both sides by (11) does not violate the equality. Still, taking Theorem 1, the separability and rotation invariance of Gaussian functions into account, we can draw the central conclusion that rotation invariants of Gaussian–Hermite moments have the same constructing formations as those of rotation invariants of geometric moments in 3D space. More formally, this conclusion can be formulated as follows:

Theorem 2. *If* χ *is a rotation invariant in geometric moments*

$$\chi\left(m^{\alpha\beta\gamma}_{p_1q_1r_1}, m^{\alpha\beta\gamma}_{p_2q_2r_2}, \ldots, m^{\alpha\beta\gamma}_{p_iq_ir_i}\right) = \chi\left(m_{p_1q_1r_1}, m_{p_2q_2r_2}, \ldots, m_{p_iq_ir_i}\right) \quad (12)$$

then χ *is also a rotation invariant in Gaussian–Hermite moments, i.e.,*

$$\chi\left(\overline{\eta}^{\alpha\beta\gamma}_{p_1q_1r_1}, \overline{\eta}^{\alpha\beta\gamma}_{p_2q_2r_2}, \ldots, \overline{\eta}^{\alpha\beta\gamma}_{p_iq_ir_i}\right) = \chi\left(\overline{\eta}_{p_1q_1r_1}, \overline{\eta}_{p_2q_2r_2}, \ldots, \overline{\eta}_{p_iq_ir_i}\right). \quad (13)$$

The proof of Theorem 2 is given in Appendix B.

Theorem 2 offers a straightforward efficient way of deriving rotation invariants from Gaussian–Hermite moments. We just take the existing invariants from geometric moments and just replace the geometric moments by the Gaussian–Hermite ones. The form of the invariants does not change at all. In this way we obtain the Gaussian–Hermite invariants "for free", without any additional investment. For example, $I_1 = \mu_{200} + \mu_{020} + \mu_{002}$ and $I_2 = \mu^2_{200} + \mu^2_{020} + \mu^2_{002} + 2\mu^2_{110} + 2\mu^2_{101} + 2\mu^2_{011}$ are the first two rotation invariants from [11,21]. According to Theorem 2, we replace every geometric moment by the corresponding Gaussian–Hermite moment in these invariants and then we obtain three rotation invariants of Gaussian–Hermite moments. For example, the first rotation invariant from Gaussian–Hermite moments is $\Phi_1 = \overline{\eta}_{200} + \overline{\eta}_{020} + \overline{\eta}_{002}$. It is possible to use all invariants presented in [21] to build the invariants of Gaussian–Hermite moments. Obviously, we can easily obtain totally 1185 rotation invariants of orthogonal Gaussian–Hermite moments. Hence, we found an efficient and elegant way of deriving orthogonal moment invariants in 3D of any orders based on Gaussian–Hermite moments. This forms the major theoretical contribution of the paper. In the next section, we demonstrate the invariance property both on artificial and real data and, namely, show the better numerical stability of Gaussian–Hermite invariants.

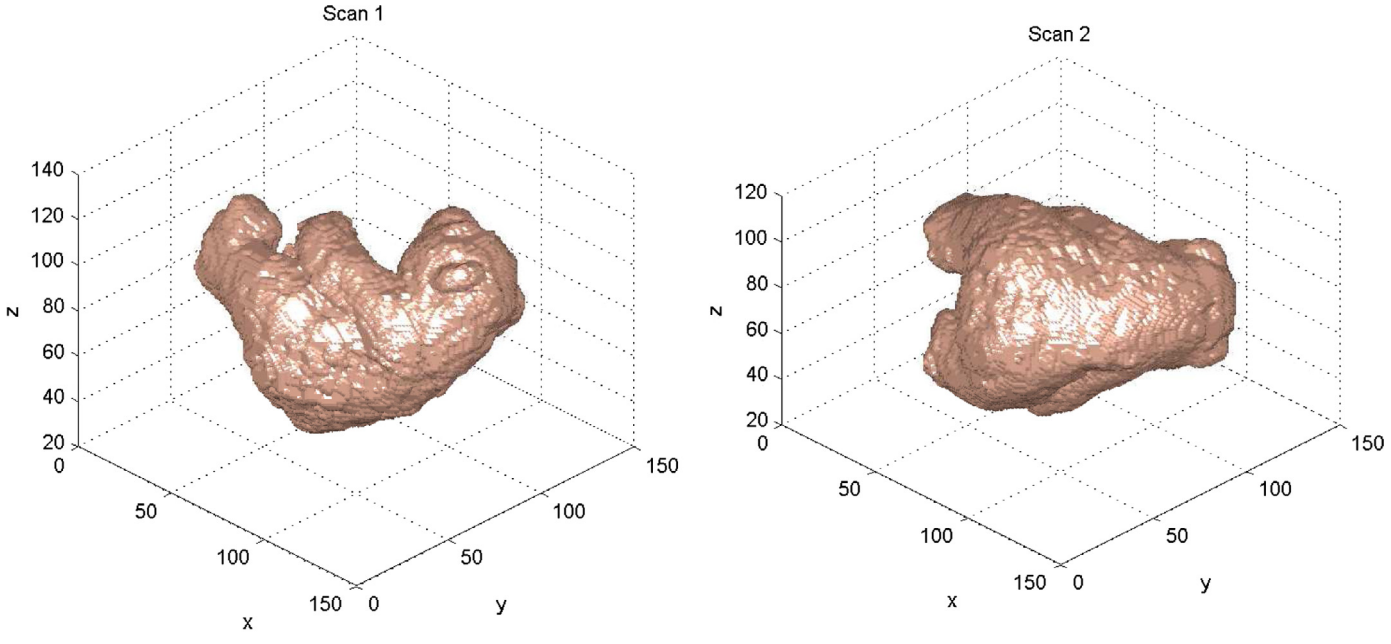

(a) The first scan (b) The second scan

Fig. 2. Two scans of a teddy bear.

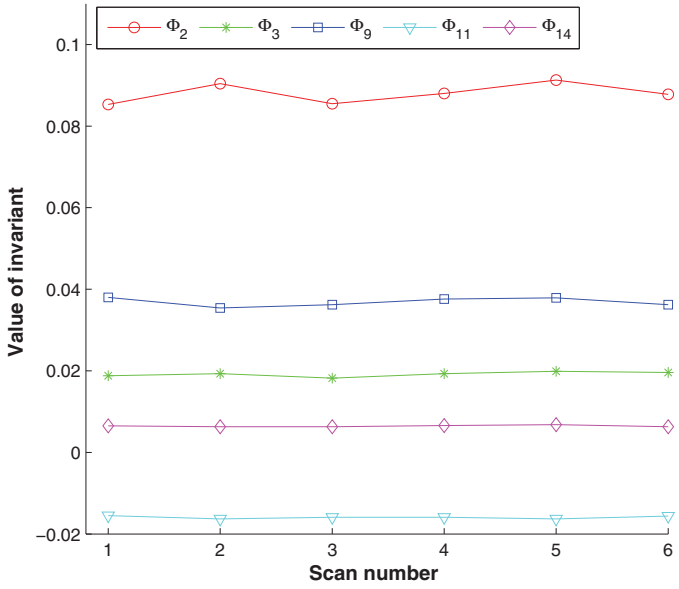

Fig. 3. The values of five selected invariants of the teddy bear. The MREs of the invariants over six rotations are 3.8%, 3.8%, 3.6%, 3.5%, and 2.9%, respectively.

4. Numerical experiments

In this section, we will test the proposed invariants numerically. We construct rotation invariants of Gaussian–Hermite moments from Φ_1 to Φ_{1185} according to those of geometric moments from I_1 to I_{1185} listed in [21]. The experiments are designed to verify rotation invariance and evaluate the numerical stability of the proposed invariants.

4.1. Verification of invariance on synthetic images

This experiment was designed to verify the rotation invariance of the proposed invariants. We used 100 objects from the Princeton Shape Benchmark (PSB) [22]. For each shape we rasterized this mesh model and inscribed it into $200 \times 200 \times 200$ volume, which was taken as the original image. This original image has only two values in its voxels: 1 for the voxels of the object and 0 for those of the background. Five random rotations of the original image were generated and the first 42 Gaussian–Hermite invariants were calculated for both original image and its rotated versions. To evaluate quantitatively the invariance, we used mean relative error (MRE) to measure the computational error of the ith invariant. The MRE of the ith invariant is defined as

$$\mathrm{MRE}_i = \frac{1}{N}\sum_{j=1}^{N}\left|\frac{\Phi_i^j - \Phi_i}{\Phi_i}\right| \times 100\%, \tag{14}$$

where Φ_i and Φ_i^j are the ith invariants of the original image and the jth rotated version, respectively. N is the number of rotated versions. Consequently, we found the maximum MRE (MMRE) for each object. MMREs of 85 objects are below 1% and that of 10 objects between 1% and 2%. In the remaining five cases, the invariant value in the denominator is so close to zero that the MMRE is higher. Anyway, this experiment exhaustively demonstrated a desirable rotation invariance.

4.2. Verification of invariance on real images

We carried out a similar experiment in more challenging conditions – we used real 3D object and its real rotations in the space. We took a teddy bear and scanned it by means of Kinect device, then we repeated this process five times with different orientations of the teddy bear in the space. Hence, we obtained six 3D scans differing from each other by rotation and also slightly by scale, quality of details and perhaps by some random errors (see Fig. 2 for two sample scans). When using Kinect, one has to scan the object from several views and Kinect software then produces a triangulated surface of the object. We converted each teddy bear figure into 3D volumetric representation of the size approximately $150 \times 150 \times 150$ voxels. Then we calculated the 14 invariants from Φ_1 to Φ_{14} of each scan. In Fig. 3 we show five randomly selected invariants computed from the different scans. As can be seen from this figure, the values of the invariants have only slight variance (check the MRE values in the figure caption), which demonstrates the desirable invariance in a real

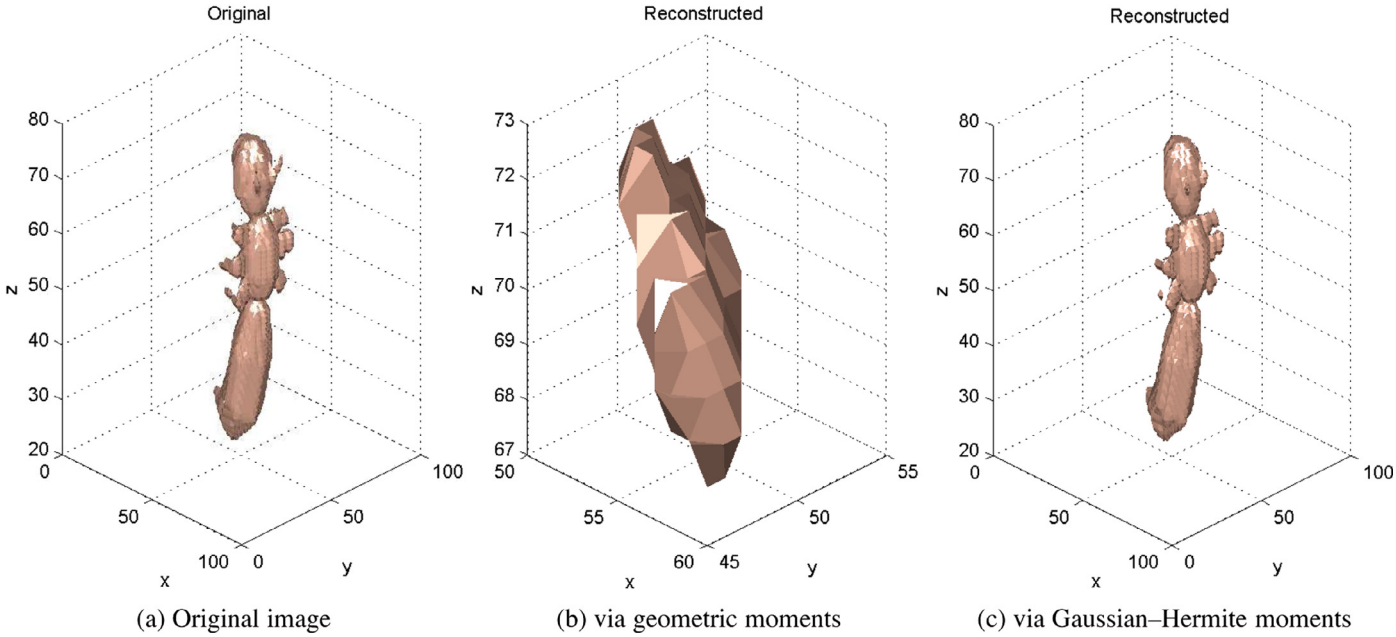

Fig. 4. The reconstruction of a volumetric image by both geometric moments (error 7336) and Gaussian–Hermite moments (error 29) using moments of orders from (0, 0, 0) to (87, 87, 87).

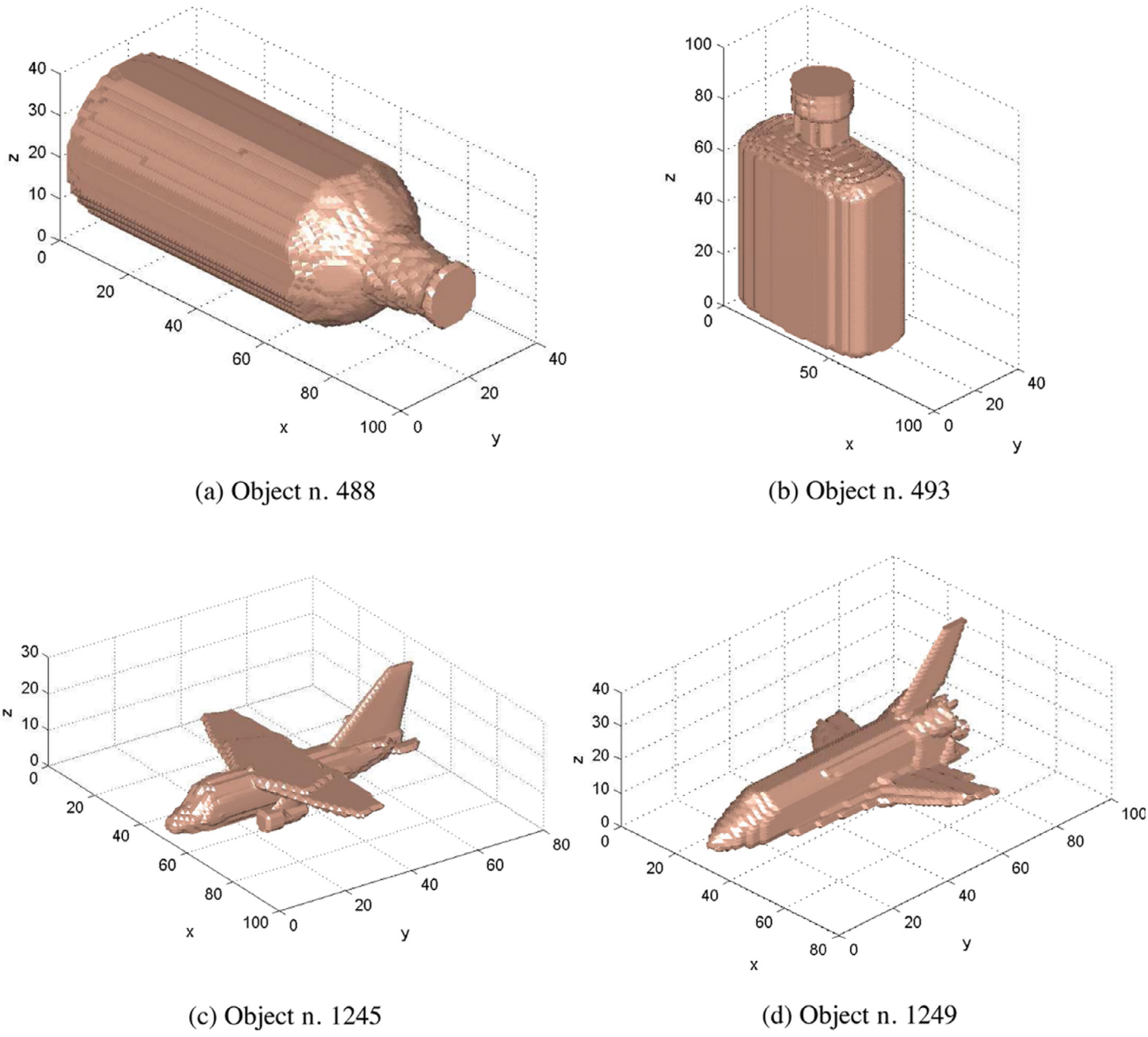

Fig. 5. The volumetric versions of the objects from PSB. (a), (b) The bottles, (c), (d) the fighter jets.

environment. The behavior of the other nine invariants is basically the same.

Comparing to the simulated case, now the MREs of individual invariants are about 10 times higher (but still safely below 5%). This does not contradict the theory but rather illustrates the problems we face when using real data acquired by a non-ideal scanner.

4.3. Image reconstruction

This experiment illustrates the major result of the paper. We show that Gaussian–Hermite moments demonstrate better image representation ability than the geometric moments. All polynomial bases of the same order are theoretically equivalent – knowing the coordinates (moments) in one of them, we can calculate the moments in the others. This works in theory but in numerical implementation we face different properties of different polynomial systems that affect their representation ability. The quality of image representation is best measured by a reconstruction error.

The direct reconstruction from the geometric moments can be computed approximately up to $10 \times 10 \times 10$ voxels only, then the kernel functions $x^p y^q z^r$ lose their precision and the whole algorithm collapses. To overcome this, the reconstruction through the Fourier transformation is commonly used

$$F(u,v,w) = \sum_{p=0}^{\infty}\sum_{q=0}^{\infty}\sum_{r=0}^{\infty} \frac{(-2\pi i)^{p+q+r}}{p!q!r!} \left(\frac{u}{N}\right)^p \left(\frac{v}{N}\right)^q \left(\frac{w}{N}\right)^r m_{pqr}. \quad (15)$$

In practice, the infinite series must be truncated. We can compute the Fourier transformation from the moments by (15) and then obtain the original image by inverse Fourier transformation. The main problem of this method is that the power series is only an approximation of the exponential kernel of the Fourier transformation. Even if we take relatively high number of moments, the error of this approximation (namely of the high-frequency parts) is still significant. Reconstruction from Gaussian–Hermite moments can be performed directly thanks to the orthogonality:

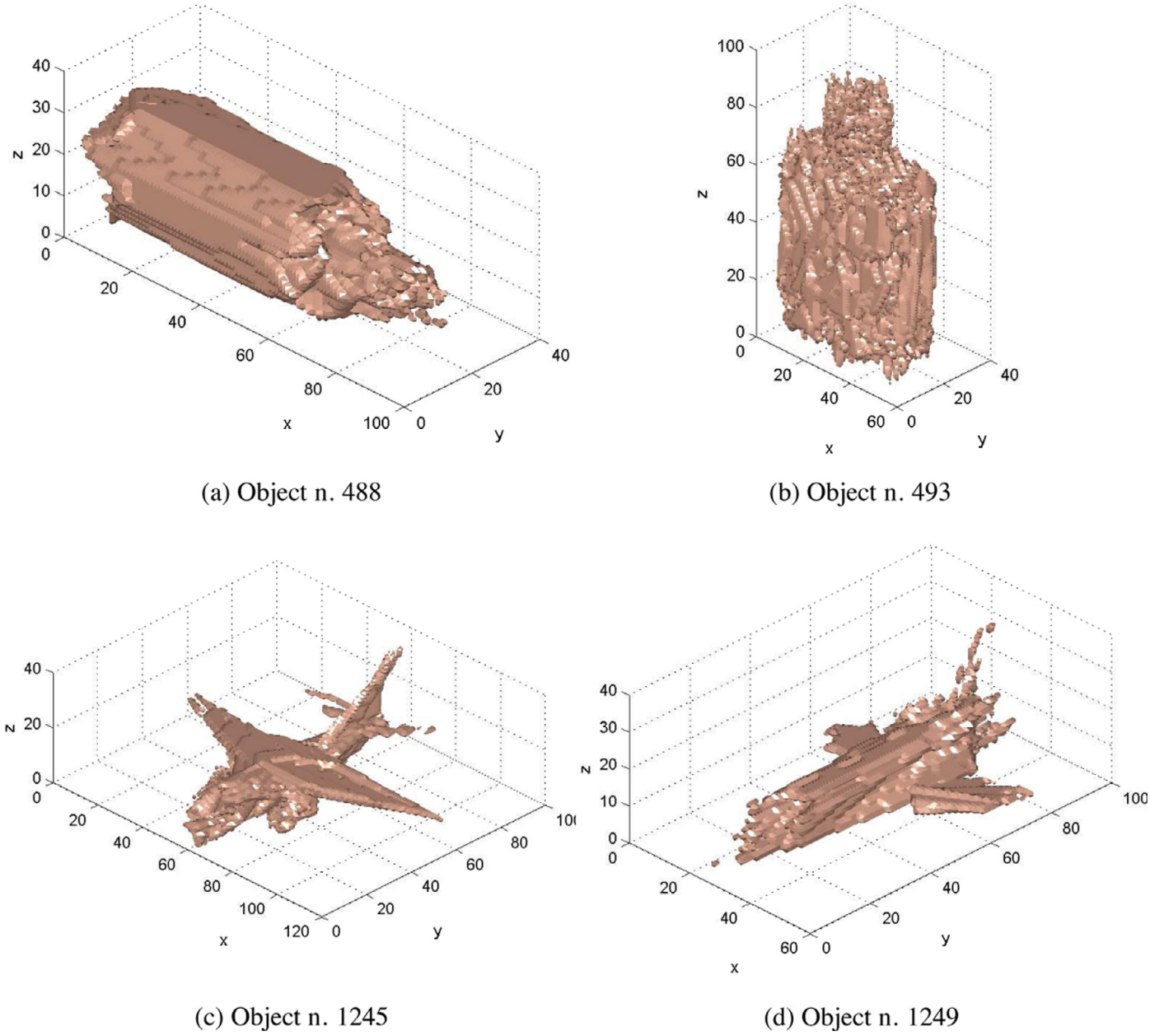

Fig. 6. The noisy (15 dB) versions of the objects from PSB. (a), (b) The bottles, (c), (d) the fighter jets.

$$f(x,y,z) = \pi^{-\frac{3}{4}}\sigma^{-\frac{3}{2}} \sum_{p=0}^{\infty}\sum_{q=0}^{\infty}\sum_{r=0}^{\infty} (2^{p+q+r}p!q!r!)^{-\frac{1}{2}}\eta_{pqr}\widetilde{H}_p(x;\sigma)$$
$$\widetilde{H}_q(y;\sigma)\widetilde{H}_r(z;\sigma) \quad x,y,z = 0,1,2,\ldots,N-1. \tag{16}$$

In discrete case, it is suitable to truncate the infinite series so the number of moments equals the number of voxels or even more, when they are not precise.

Hence, there is neither an ill-conditioned problem nor inaccurate use of Fourier transformation. As we can see in the experiment, this results in much better reconstruction. We used a binary volumetric image of the size $100 \times 100 \times 100$ voxels of an insect (see Fig. 4a) from the Princeton database. We calculated both geometric and Gaussian–Hermite moments of it up to the order 87. This is the maximum achievable order for geometric moments; higher-order moments are subject of floating-point overflow. Gaussian–Hermite moments could be calculated up to higher orders but we used the same order as for geometric moments to keep the comparison unbiased. The reconstruction from geometric moments via Fourier transformation is of a poor quality with all fine details degraded (see Fig. 4b). On the other hand, the reconstruction from Gaussian–Hermite moments contains almost all fine parts such as the claws, the feelers, and the butt quite vividly apparent, see Fig. 4c. The reconstruction quality can be quantified by the number of different voxels between the reconstructed image and the original. The error of the reconstruction from geometric moments is 7336, while Gaussian–Hermite moments yield almost negligible error equal to 29. This result clearly demonstrates that Gaussian–Hermite moments provide significantly better image representation than geometric moments in 3D case. Hence, 3D invariants based on Gaussian–Hermite moments have better discrimination ability than 3D geometric invariants.

4.4. Object recognition

In this experiment we demonstrate that the better numerical stability of the Gaussian–Hermite moments actually increases the

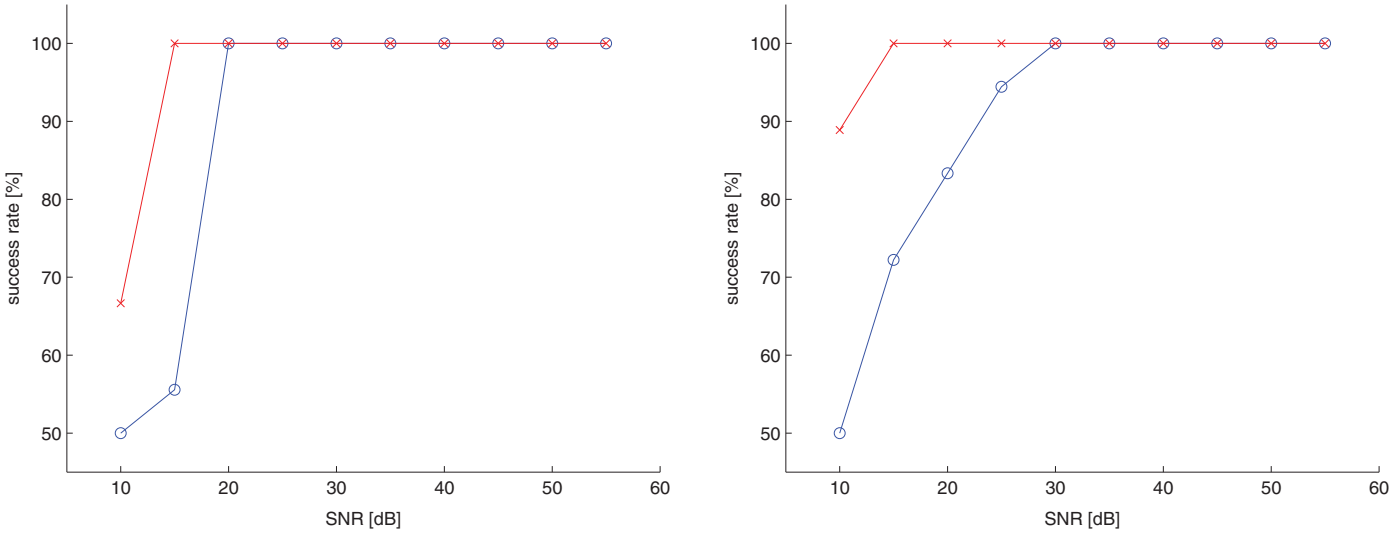

(a) Bottles (b) Fighter jets

Fig. 7. The success rate of the recognition. (a) The bottles, (b) the fighter jets. Legend: −○− geometric moments, −×− Gaussian–Hermite moments.

recognition power of the respective invariants in some cases. We again used the objects from the Princeton Shape Benchmark [22]. To demonstrate the phenomenon, we selected several pairs of objects that are visually very similar to each other (see Fig. 5 for two examples). For each object we generated 90 "shaky" instances by adding a zero-mean Gaussian noise to the coordinates of the triangle vertices of the object surface (see Fig. 6). The amount of the noise was measured by the signal-to-noise ratio (SNR), defined in this case as

$$\mathrm{SNR} = 10 \log \left(\sigma_s^2/\sigma_n^2\right), \tag{17}$$

where σ_s is the standard deviation of the object coordinates and σ_n is the standard deviation of the noise. We used SNRs from 55dB to 10dB, so we had nine degraded instances on each noise level. Now we let the algorithm to recognize the shaky objects by means of the geometric invariants I_{1181}, I_{1182}, I_{1183}, I_{1184}, and I_{1185} [21] and by the corresponding Gaussian–Hermite invariants Φ_{1181}, Φ_{1182}, Φ_{1183}, Φ_{1184}, and Φ_{1185}. We intentionally used these higher-order invariants (from 13th to 16th order) because low-order invariants either cannot distinguish similar objects or, if they can, they do not suffer by the loss of precision in case of geometric moments.

The success curves of the objects from Fig. 5 are shown in Fig. 7. If the noise is mild, both invariants can recognize the objects perfectly. On medium levels of noise, the performance of the Gaussian–Hermite invariants dominates. The explanation is in numerical stability – geometric moments of orders 13–16 lose the precision due to the necessity of working with very high values while Gaussian–Hermite moments can be computed in a stable way with much less precision loss. For a heavy noise 10dB, the shaky objects are so similar that the performance of both methods decreases. However, the performance of the Gaussian–Hermite invariants is still in the range 65–90% while that of the geometric invariants drops to 50%, which is in the case of two classes equal to a random decision. This experiment clearly illustrates the advantage of Gaussian–Hermite invariants when recognizing similar objects. If the objects (classes) are significantly different, they can be discriminated by low-order invariants and the described effect does not show up.

5. Conclusion

In this paper, we proposed an approach to developing 3D rotation invariants based on orthogonal Gaussian–Hermite moments. We have found an important rotation property of Hermite polynomials and used it to construct the invariants. The rotation invariants of Gaussian–Hermite moments in 3D space have the same formations as those of geometric rotation invariants. This is a significant theoretical result, because it offers the solution to the problem of developing 3D rotation invariants from Gaussian–Hermite moments both theoretically and practically. With this result, we can construct the rotation invariants of Gaussian–Hermite moments from the existing geometric rotation invariants. It is no longer necessary to derive rotation invariants based on Hermite polynomials or basis functions directly "from scratch".

The actual calculation of the Gaussian–Hermite moments is then performed by means of recurrent relations, which avoids the unstable calculation of geometric moments. Experimental results on both synthetic and real data verified the rotation invariance of Gaussian–Hermite invariants. At the same time, the superior numerical stability of Gaussian–Hermite moments and invariants was confirmed compared to traditional invariants from geometric moments by experiments with object reconstruction and with recognition of noisy shapes.

Acknowledgments

The authors thank the Czech Science Foundation for financial support of this work under the grant number P103/11/1552. B. Yang was also supported by the ERCIM "Alain Bensoussan" Fellowship Programme (financed by the Marie Curie Co-funding of Regional, National, and International Programmes of the European Commission) and by the post-doctoral fellowship of the Academy of Sciences of the Czech Republic.

Appendix A. Proof of Theorem 1

Suppose the original coordinates are (x, y, z). After the rotation along z axis by angle α, the transitional coordinates $(\tilde{x}, \tilde{y}, \tilde{z})$ are determined by

$$(\tilde{x}\ \tilde{y}\ \tilde{z})^T = \mathbf{R_z}(\alpha)\,(x\ y\ z)^T. \tag{A.1}$$

The subsequent rotation along y axis by angle $-\beta$ creates the transitional coordinates $(\bar{x}, \bar{y}, \bar{z})$, which can be calculated from the previous coordinates $(\tilde{x}, \tilde{y}, \tilde{z})$ as

$$(\bar{x}\ \bar{y}\ \bar{z})^T = \mathbf{R_y}(-\beta)\,(\tilde{x}\ \tilde{y}\ \tilde{z})^T. \tag{A.2}$$

The third rotation along x axis by angle γ produces the coordinates $(\hat{x}, \hat{y}, \hat{z})$

$$(\hat{x}\ \hat{y}\ \hat{z})^T = \mathbf{R_x}(\gamma)\,(\bar{x}\ \bar{y}\ \bar{z})^T. \tag{A.3}$$

According to (A.3) and Theorem 1 in [19] we have

$$\begin{aligned}\hat{x}^p\hat{y}^q\hat{z}^r &= \bar{x}^p(\bar{y}\cos\gamma - \bar{z}\sin\gamma)^q(\bar{y}\sin\gamma + \bar{z}\cos\gamma)^r \\ &= \sum_{s=0}^{q+r} k(s,q,r,\gamma)\bar{x}^p\bar{y}^{q+r-s}\bar{z}^s,\end{aligned} \tag{A.4}$$

and

$$\begin{aligned}H_p(\hat{x})H_q(\hat{y})H_r(\hat{z}) &= H_p(\bar{x})H_q(\bar{y}\cos\gamma - \bar{z}\sin\gamma)H_r(\bar{y}\sin\gamma + \bar{z}\cos\gamma) \\ &= \sum_{s=0}^{q+r} k(s,q,r,\gamma)\,H_p(\bar{x})H_{q+r-s}(\bar{y})H_s(\bar{z}).\end{aligned} \tag{A.5}$$

Substituting (A.2) into (A.4) and (A.5), (A.4) can be further expanded as

$$\begin{aligned}&\sum_{s=0}^{q+r} k(s,q,r,\gamma)(\tilde{x}\cos\beta + \tilde{z}\sin\beta)^p(-\tilde{x}\sin\beta + \tilde{z}\cos\beta)^s\tilde{y}^{q+r-s} \\ &= \sum_{s=0}^{q+r} k(s,q,r,\gamma)\sum_{t=0}^{p+s} k(t,p,s,-\beta)\tilde{x}^{p+s-t}\tilde{y}^{q+r-s}\tilde{z}^t\end{aligned} \tag{A.6}$$

and (A.5) is also expanded as

$$\begin{aligned}&\sum_{s=0}^{q+r} k(s,q,r,\gamma)H_p(\tilde{x}\cos\beta + \tilde{z}\sin\beta)H_s(-\tilde{x}\sin\beta + \tilde{z}\cos\beta)H_{q+r-s}(\tilde{y}) \\ &= \sum_{s=0}^{q+r} k(s,q,r,\gamma)\sum_{t=0}^{p+s} k(t,p,s,-\beta)H_{p+s-t}(\tilde{x})H_{q+r-s}(\tilde{y})H_t(\tilde{z}).\end{aligned} \tag{A.7}$$

After substituting (A.1) into (A.6) and (A.7), (A.6) has the form

$$\begin{aligned}&\sum_{s=0}^{q+r} k(s,q,r,\gamma)\sum_{t=0}^{p+s} k(t,p,s,-\beta)(x\cos\alpha - y\sin\alpha)^{p+s-t} \\ &\times(x\sin\alpha + y\cos\alpha)^{q+r-s}z^t = \sum_{s=0}^{q+r} k(s,q,r,\gamma)\sum_{t=0}^{p+s} k(t,p,s,-\beta) \\ &\times \sum_{u=0}^{p+q+r-t} k(u,p+s-t,q+r-s,\alpha)x^{p+q+r-t-u}y^u z^t\end{aligned} \tag{A.8}$$

and (A.7) becomes

$$\begin{aligned}&\sum_{s=0}^{q+r} k(s,q,r,\gamma)\sum_{t=0}^{p+s} k(t,p,s,-\beta)H_{p+s-t}(x\cos\alpha - y\sin\alpha) \\ &H_{q+r-s}(x\sin\alpha + y\cos\alpha)H_t(z) = \sum_{s=0}^{q+r} k(s,q,r,\gamma)\sum_{t=0}^{p+s} k(t,p,s,-\beta) \\ &\times \sum_{u=0}^{p+q+r-t} k(u,p+s-t,q+r-s,\alpha)\,H_{p+q+r-t-u}(x)H_u(y)H_t(z).\end{aligned} \tag{A.9}$$

(A.8) indicates a linear combination. Substantially, it can be rewritten to

$$\hat{x}^p\hat{y}^q\hat{z}^r = \sum_{i=1}^{L(p,q,r)} \mathrm{con}_i\,(p,q,r,\alpha,\beta,\gamma)\,x^{p_i}y^{q_i}z^{r_i}. \tag{A.10}$$

Likewise, (A.9) can be also rewritten to

$$H_p(\hat{x})H_q(\hat{y})H_r(\hat{z}) = \sum_{i=1}^{L(p,q,r)} \mathrm{con}_i\,(p,q,r,\alpha,\beta,\gamma)\,H_{p_i}(x)H_{q_i}(y)H_{r_i}(z) \tag{A.11}$$

The proof of Theorem 1 has been completed.

Appendix B. Proof of Theorem 2

Suppose we have the original image $f(x,y,z)$ defined in V and the rotated image $f^R(\hat{x},\hat{y},\hat{z})$ defined in V^R. After the rotation, the geometric moment of order $(p+q+r)$ for $f^R(\hat{x},\hat{y},\hat{z})$ is defined as

$$m_{pqr}^{\alpha\beta\gamma} = \iiint_{V^R} \hat{x}^p\hat{y}^q\hat{z}^r f^R(\hat{x},\hat{y},\hat{z})d\hat{x}d\hat{y}d\hat{z}. \tag{B.1}$$

After the substitution $(\hat{x}\ \hat{y}\ \hat{z})^T = \mathbf{R}(x\ y\ z)^T$ and considering that $f^R(\hat{x},\hat{y},\hat{z}) = f(x,y,z)$ we get

$$\begin{aligned}m_{pqr}^{\alpha\beta\gamma} &= \iiint_V \hat{x}^p\hat{y}^q\hat{z}^r f(x,y,z)|J|dxdydz \\ &= \sum_{i=1}^{L(p,q,r)} con_i\,(p,q,r,\alpha,\beta,\gamma)\,m_{p_iq_ir_i},\end{aligned} \tag{B.2}$$

where $|J| = \det(\mathbf{R}^T) = 1$. When σ in (7) has the same value for x, y and z axes, Gaussian–Hermite moments can be computed in a similar way

$$\begin{aligned}\eta_{pqr}^{\alpha\beta\gamma} &= \iiint_{V^R} \widehat{H}_p(\hat{x})\widehat{H}_q(\hat{y})\widehat{H}_r(\hat{z})f^R(\hat{x},\hat{y},\hat{z})d\hat{x}d\hat{y}d\hat{z} \\ &= \iiint_V \widehat{H}_p(\hat{x})\widehat{H}_q(\hat{y})\widehat{H}_r(\hat{z})f(x,y,z)|J|dxdydz \\ &= \sum_{i=1}^{L(p,q,r)} con_i(p,q,r,\alpha,\beta,\gamma)\eta_{p_iq_ir_i}.\end{aligned} \tag{B.3}$$

Let χ be a rotation invariant of geometric moments that has a form of (12). Since it is an invariant, the angles α, β, γ are completely eliminated. Therefore, according to (B.2), (B.3), and (12), the combination χ also eliminates the angles in Gaussian–Hermite moments,

$$\chi\left(\eta_{p_1q_1r_1}^{\alpha\beta\gamma}, \eta_{p_2q_2r_2}^{\alpha\beta\gamma}, \cdots, \eta_{p_iq_ir_i}^{\alpha\beta\gamma}\right) = \chi\left(\eta_{p_1q_1r_1}, \eta_{p_2q_2r_2}, \cdots, \eta_{p_iq_ir_i}\right) \tag{B.4}$$

In order to obtain the translation invariance simultaneously, $\eta_{p_iq_ir_i}$ in (B.4) can be correspondingly replaced by $\overline{\eta}_{p_iq_ir_i}$, which then establishes (13). The proof of Theorem 2 has been completed.

References

[1] J. Flusser, T. Suk, B. Zitová, Moments and Moment Invariants in Pattern Recognition, Wiley, 2009.
[2] F.A. Sadjadi, E.L. Hall, Three-dimensional moment invariants, IEEE Trans. Pattern Anal. Mach. Intell. PAMI-2 (1980) 127–136.
[3] X. Guo, Three dimensional moment invariants under rigid transformation, in: Proceedings of the Fifth International Conference on Computer Analysis of Images and Patterns (CAIP'93), 1993, pp. 518–522.
[4] D. Cyganski, J.A. Orr, Object Recognition and Orientation Determination by Tensor Methods, JAI Press, 1988.
[5] T.H. Reiss, Recognizing Planar Objects Using Invariant Image Features, first ed., Springer, 1993.
[6] D. Xu, H. Li, Geometric moment invariants, Pattern Recognit. 41 (2008) 240–249.
[7] J.M. Galvez, M. Canton, Normalization and shape recognition of three-dimensional objects by 3D moments, Pattern Recognit. 26(5) (1993) 667–681.
[8] M.A. Westenberg, J.B.T.M. Roerdink, M.H.F. Wilkinson, Volumetric attribute filtering and interactive visualization using the max-tree representation, IEEE Trans. Image Process. 16 (2007) 2943–2952.
[9] C.H. Lo, H.S. Don, 3-D moment forms: their construction and application to object identification and positioning, IEEE Trans. Pattern Anal. Mach. Intell. 11 (1989) 1053–1064.
[10] J. Flusser, J. Boldyš, B. Zitová, Moment forms invariant to rotation and blur in arbitrary number of dimensions, IEEE Trans. Pattern Anal. Mach. Intell. 25 (2003) 234–246.
[11] T. Suk, J. Flusser, Tensor method for constructing 3D moment invariants, in: Proceedings of the 14th International Conference on Computer Analysis of Images and Patterns (CAIP'11), 2011, pp. 212–219.
[12] R. Kakarala, D. Mao, A theory of phase-sensitive rotation invariance with spherical harmonic and moment-based representations, in: IEEE Conference on Computer Vision and Pattern Recognition CVPR'10, 2010, pp. 105–112.
[13] M. Kazhdan, An approximate and efficient method for optimal rotation alignment of 3D models, IEEE Trans. Pattern Anal. Mach. Intell. 29 (7) (2007) 1221–1229.
[14] M. Kazhdan, T. Funkhouser, S. Rusinkiewicz, Rotation invariant spherical harmonic representation of 3D shape descriptors, in: Proceedings of the 2003 Eurographics/ACM SIGGRAPH Symposium on Geometry Processing, SGP'03, Eurographics Association, 2003, pp. 156–164.

[15] J. Fehr, Local rotation invariant patch descriptors for 3D vector fields, in: Proceedings of the 20th International Conference on Pattern Recognition ICPR'10, IEEE Computer Society, 2010, pp. 1381–1384.
[16] J. Fehr, H. Burkhardt, 3D rotation invariant local binary patterns, in: Proceedings of the 19th International Conference on Pattern Recognition ICPR'08, IEEE Computer Society, 2008, pp. 1–4.
[17] H. Skibbe, M. Reisert, H. Burkhardt, SHOG-spherical HOG descriptors for rotation invariant 3D object detection, in: R. Mester, M. Felsberg (Eds.), Deutsche Arbeitsgemeinschaft für Mustererkennung DAGM'11, Lecture Notes in Computer Science, vol. 6835, Springer, 2011, pp. 142–151.
[18] N. Canterakis, 3D Zernike moments and Zernike affine invariants for 3D image analysis and recognition, in: Proceedings of the 11th Scandinavian Conference on Image Analysis SCIA'99, DSAGM, 1999, pp. 85–93.
[19] B. Yang, G.X. Li, H.L. Zhang, M. Dai, Rotation and translation invariants of Gaussian–Hermite moments, Pattern Recognit. Lett. 32 (2011) 1283–1298.
[20] H. Goldstein, C. Poole, J. Safko, Classical Mechanics, 3rd ed., Addison-Wesley, 2001.
[21] T. Suk, J. Flusser, 3D rotation invariants, http://zoi.utia.cas.cz/3DRotationInvariants, 2012.
[22] Princeton, Princeton Shape Benchmark, http://shape.cs.princeton.edu/benchmark/, 2013.